Review Paper

ISSN 1225-6153
Online ISSN 2287-8955

Numerical Studies on Submerged Arc Welding Process

Degala Ventaka Kiran* and Suck-Joo Na*,†

*Department of Mechanical Engineering, KAIST, Daejeon 305-701, Korea

†Corresponding author : sjoona@kaist.ac.kr

(Received June 9, 2014 ; Accepted August 4, 2014)

Abstract

A quantitative understanding on the effect of the welding conditions on weld joint dimensions and weld thermal cycle is difficult through experimental studies alone. The experimental realization of temperature distribution in the weld pool is proved to be extremely difficult due to the small size of welds, high peak temperature and steep temperature gradients in weld pool. This review deals with the heat transfer and fluid flow analysis to understand the parametric influence of a single wire submerged arc welding (SAW) and multi-wire SAW processes on the weld bead dimensions, temperature and fluid flow distribution in the weldment.

Key Words : Submerged arc welding process, Heat transfer and fluid flow analysis, Tandem submerged arc welding process.

1. Introduction

Numerical modeling of heat transfer and fluid flow phenomenon has been successfully used for the estimation of peak temperature and thermal cycle in fusion welding processes[1]. In many cases, the computed thermal cycles are used to predict the final microstructure and mechanical properties of the weld. The typical nature of the submerged arc welding (SAW) process makes it difficult to measure peak temperature and thermal cycles in the weld experimentally. In particular, the two wire submerged arc welding (SAW-T) process provides a greater difficulty due to the application of two welding arcs and its associated numerous parameters, and use of greater amount of fluxes.

In this paper, a comprehensive literature review on the numerical modeling of the SAW and SAW-T processes to understand the influence of process parameters on the weld bead dimensions, temperature distribution in the weldment are presented.

2. Theoretical modeling

2.1. Heat transfer analysis

Pathak et al.[2] proposed a finite element based conduction heat transfer model to analyze single wire SAW process. A Gaussian distributed surface heat source is used to simulate the heat transfer from the welding arc (Fig. 1). The Gaussian distributed surface heat source is given by the eq. (1).

$$q(r) = \frac{\eta VI}{2\pi\sigma^2} \exp\left(\frac{-(x^2+y^2)}{2\sigma^2}\right) \quad (1)$$

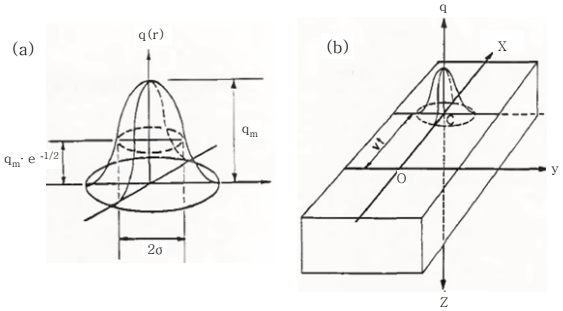

Fig. 1 (a) Gaussian distributed surface heat source (b) position of the moving heat source after time t (s)[2]

where the terms η, V, I and σ refer to the process efficiency, welding voltage and current, and the effective arc radius. Around 68% of the arc energy is distributed over the area covered with in 2σ. Based on some numerical results and the corresponding comparison with the experimental results it was proposed that the effective arc radius (σ) was 2.1 times that of the measured half bead width. However the filler metal deposition was not modeled effectively. Mahapatra et al.[3] reported a similar model using "*element deactivation and activation*" approach to account for the addition of filler materials. Fig. 2(a) depict the modeling of the filler material deposition using this approach. The elements defining the weld pool region were divided into sets such that these elements remain deactivated initially. These deactivated elements were assigned with very low values of thermal conductivity so that these elements would have little impact on the heat transfer calculations. At every step, a selected set of the deactivated elements was activated, which involved reassigning of original material properties to these elements, as the heat source moved along the weld interface. The computed and measured weld pool shapes and the thermal cycles in HAZ were reported to be in fair agreement. Biswas et al.[4] followed a similar approach in modeling double-sided fillet welding using single wire SAW process.

The conduction heat transfer based weld pool simulation often fails to account for the convective transport of heat inside the pool, which can be significant, in particular, for a large weld pool generated in SAW process. Goldak et al. [5] introduced a double-ellipsoidal volumetric heat source model to numerically account for the heat transport inside the weld pool in a conduction based heat transfer analysis. The double-ellipsoid heat source was obtained as a combination of two ellipsoids - one in the front and the other at the rear with reference to the center of the welding arc [Fig. 2 (b)]. The power density distributions in the front and at the rear of the double-ellipsoidal heat sources are given as[5]

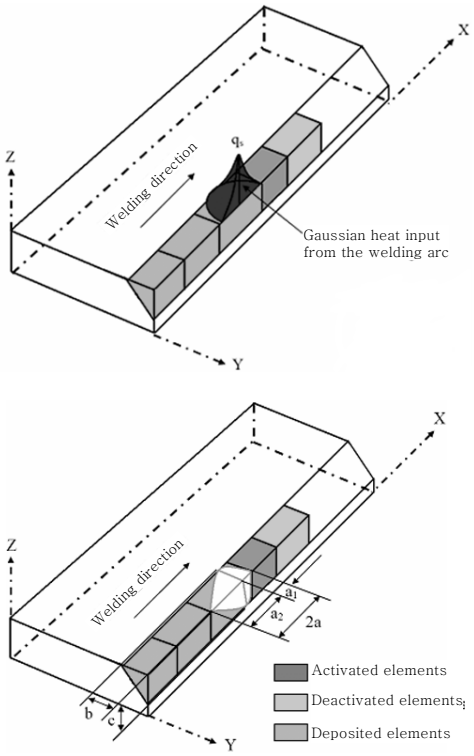

Fig. 2 (a) Schematic representation of the Gaussian distributed heat source and the element deactivation and activation methodology[3], (b) double ellipsoidal volumetric heat source[5]

$$\dot{Q} = \frac{6\sqrt{3}\, f_1\, P\, \eta}{\pi\sqrt{\pi}\, a_1\, b\, c} \exp\left(-\frac{3x^2}{a_1^2} - \frac{3y^2}{b^2} - \frac{3z^2}{c^2} \right) \quad (2)$$

$$\dot{Q} = \frac{6\sqrt{3}\, f_2\, P\, \eta}{\pi\sqrt{\pi}\, a_2\, b\, c} \exp\left(-\frac{3x^2}{a_2^2} - \frac{3y^2}{b^2} - \frac{3z^2}{c^2} \right) \quad (3)$$

where the terms a_1, b, and c refer to the semi major axis, minor axis and depth of the front semi-ellipsoid, respectively, and that of the rear semi-ellipsoid is denoted as a_2, b, and c. The fractions f_1 and f_2 are used to consider the asymmetry in the magnitude of heat energy density in the front and at the rear part of the heat sources. The values of f_1 and f_2 are suggested as 0.6 and 1.4, respectively, in open literatures[5-8]. However, it is very difficult to decide the appropriate dimensions of the double-ellipsoidal heat source. Very often these were defined based on the experimentally measured weld bead macrographs.

Sharma et al.[9] estimated the dimensions of

the double-ellipsoidal heat source of twin arc SAW process by numerical experiments and its validation with the measured weld bead dimensions. The author assumed that the close proximity of the two arcs leads to a single arc. Kiran et al.[10] presented a 3D conduction heat transfer model of the SAW-T process. The leading and trailing wires are connected to DCEP and variable polarity AC power sources. The model considers two individual volumetric heat sources to account for heat input from the leading and the trailing arcs. The power density distributions of the leading and trailing double-ellipsoidal heat sources are presented by a generic expression as[10]

$$\dot{Q}_i = \frac{6\sqrt{3}\, f_i\, P_i}{\pi\sqrt{\pi}\, a_i\, b_i\, c_i} \exp\left(-\frac{3x^2}{a_i^2} - \frac{3y^2}{b_i^2} - \frac{3z^2}{c_i^2}\right) \quad (4)$$

where the subscript i refers to either leading (i ≡ LE) or trailing (i ≡ TR) arc or heat source. The power from the leading arc to the work piece (P_{LE}) is computed as

$$P_{LE} = \eta\ \alpha\ V_{LE}\ I_{LE} \quad (5)$$

where η is the process efficiency and α is the fraction of the available arc energy supplied to the work piece in direct current electrode positive (DCEP) mode. The effective current (I_{TR}) and power (P_{TR}) of the trailing arc to the workpiece are estimated respectively as

$$I_{TR} = \left[\frac{(I_{TR}^{+} t_{TR}^{+}) + (I_{TR}^{-} t_{TR}^{-})}{(t_{TR}^{+} + t_{TR}^{-})}\right]; \quad (6)$$

$$P_{TR} = \left[\eta V_{TR} \frac{(\gamma I_{TR}^{+} t_{TR}^{+}) + (\beta I_{TR}^{-} t_{TR}^{-})}{(t_{TR}^{+} + t_{TR}^{-})}\right] \quad (7)$$

In eq. (7), γ and β refer to the fractional arc energy supplied to workpiece in the positive and negative current pulses, respectively. The values of both α [in eq. (5)] and γ [in eq. (7)] are taken as 0.75[11,12]. The value of β [in eq. (7)] is taken as 0.65[11,12].

Fig. 3 schematically presents the solution domain, volumetric heat sources and the electrode wire metal deposition in weld pool considered by

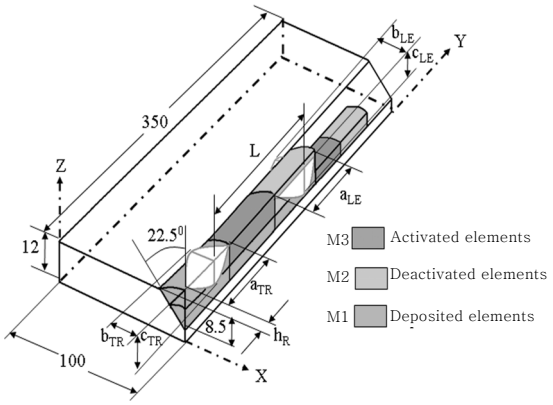

Fig. 3 Solution domain for SAW-T process numerical modeling[10]

discrete addition of new elements. A symmetrical analysis is carried out considering the weld interface along the middle of the V-groove as the symmetry plane. In Fig. 3, M1, M2 and M3 correspond to electrode material already deposited in a previous time step, yet to be deposited (i.e. deactivated elements) and deposited in the current time step (i.e. newly activated elements), respectively. Thus, elements designated as M1 and M3 are assigned with the thermo physical properties of work piece material. The M2 set of elements are assigned with very low values of thermal conductivity to mimic atmosphere (thermally insulator). A new set of elements (M3) are activated at the liquidus temperature in the beginning of each time step. The time stepping and the activation scheme of new elements are synchronized in a manner such that, two separate sets of new elements (M3) will be activated in each time step to account for the depositions from the lead and the trial wires.

A methodology was proposed to estimate the dimensions of volumetric heat sources based on weld joint geometry and process parameters as given by the eqs. (8) and (9).

$$a_{LE} = b_{LE} = \left[\frac{3}{2\pi d}\left(\frac{P_{LE}\eta_m t_s}{\rho[C_p(T_L - T_A) + L]} + U_{LE}\right)\right]^{0.5} \quad (8)$$

$$a_{TR} = b_{TR} = \left[\frac{3}{2\pi(d - h_{LE})}\left(\frac{P_{TR}\eta_m t_s}{\rho[C_p(T_L - T_A) + L]} + U_{TR}\right)\right]^{0.5} \quad (9)$$

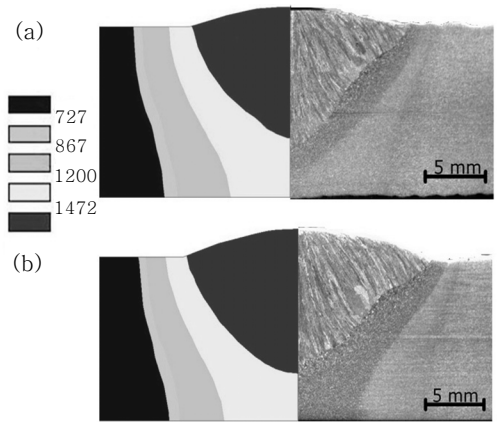

Fig. 4 Comparison of experimentally measured and corresponding computed weld pool shapes with: (a) I_{TR}^{+} = 344 A, I_{TR}^{-} = 563 A, t_{TR}^{+} = 7.11 ms, t_{TR}^{-} = 9.56 ms, and (b) I_{TR}^{+} = 344 A, I_{TR}^{-} = 797 A, t_{TR}^{+} = 5.35 ms, t_{TR}^{-} = 11.32 s[10)]

The computed weld dimensions and thermal cycles in heat affected zone (HAZ) are validated with the corresponding experimentally measured results and found to be in fair agreement [Fig. (4)]. The effect of the pulsating nature of the trail arc current on the weld dimensions, cooling rate and the mechanical properties of the weld is studied.

Kiran et al.[13)] correlated the computed weld pool cooling rate ($\Delta T_{8/5}$) with the measured values of the weld metal ferrite phases at different trailing wire currents in SAW-T process. The increase in I_{TR} reduced the cooling rates and weld microstructures showed reduction in acicular ferrite phase fraction associated with coarsening of the remaining phases like allotriomorphic ferrite. Similar relationships between the weld metal microstructure[14)] and measured acicular ferrite area fraction[15)] with cooling rates in C-Mn steels of comparable compositions were also reported earlier. Pilipinko et al.[16)] reported a 2-D and 3-D thermal models to predict the thermal cycles in long fillet and butt welds made by three-wire SAW process. The computed results were compared with the similar results computed for a single electrode wire multi-pass SAW process. The computed values of the cooling rate in the weld pool was nearly 4~10 times in the three-wire SAW processes in comparison to the same in the single electrode SAW process.

2.2 Heat transfer and fluid flow analysis

The conduction heat transfer models are unable to account for convective transport of heat, which is especially significant in large weld pool in a true sense. The convective flow in weld pool would be driven by buoyancy force, electromagnetic force (Lorentz force), the shear stress induced by the surface tension gradient at the weld pool surface, and the shear stress acting on the pool surface by the plasma jet[17)]. Cho et al.[18)] developed a three dimensional heat transfer and fluid flow model for single wire SAW process. The influence of torch angle on the fluid flow and convective heat transfer was analyzed. The model solves the governing equations like the conservation of mass, momentum and energy along with the volume of fluid method. The volume of fluid method is used to track the shape of the free surface. The molten metal was assumed to have Newtonian viscosity and incompressible laminar flow. Based on these assumptions the aforementioned governing equations are explained as

Mass conservation equation:

$$\nabla.\vec{V} = \frac{\dot{m}_s}{\rho} \tag{10}$$

Momentum equations:

$$\frac{\partial \vec{V}}{\partial t} + \vec{V}.\nabla\vec{V} = -\frac{1}{\rho}\nabla P + \nu\nabla^2\vec{V} + \frac{\dot{m}_s}{\rho}\left(\vec{V}_s - \vec{V}\right) + f_b \tag{11}$$

Energy conservation equation:

$$\frac{\partial h}{\partial t} + \vec{V}.\nabla h = \frac{1}{\rho}\nabla.(k\nabla T) + \dot{h}_s \tag{12}$$

$$h = \begin{cases} \rho_s C_s T & (T \le T_s) \\ h(T_s) + h_{sl}\left(\dfrac{T - T_s}{T_l - T_s}\right) & (T_s \le T \le T_l) \\ h(T_l) + \rho_l C_l (T - T_l) & (T_l \le T) \end{cases} \tag{13}$$

Here, h is the enthalpy, ρ_s and ρ_l are solid and liquid density, C_s and C_l are specific heat at constant volume of the solid and liquid phases, T_s and T_l are solidus and liquidus temperature, and h_{sl} is the latent heat of fusion.

VOF equation:

$$\frac{\partial F}{\partial t}+\nabla.\left(\vec{V}F\right)=\dot{F}_s \tag{14}$$

Here, F is a volume of fluid and $\dot{F}_s$ is the change of the volume fraction of fluid associated with the mass source $\dot{m}_s$ in the continuity equation. The energy and pressure boundary condition are considered as

$$\begin{aligned} k\frac{\partial T}{\partial \vec{n}} &= q_a - q_{con} - q_{rad} \\ &= q_a - h(T-T_0) - \varepsilon\sigma\left(T^4 - T_0^4\right) \end{aligned} \tag{15}$$

$$P = P_a + \frac{\gamma}{R_c} \tag{16}$$

Here, $\vec{n}$ is the vector normal to the local free surface, h is the convective heat transfer coefficient, T_0 is the ambient temperature, ε is the surface radiation emissivity, and σ is the Stefan-Boltzmann constant. The terms ɣ and R_c denote the surface tension coefficient and the radius of the surface curvature, respectively.

The heat source of the electric arc [eq. (15)] can be modeled as a surface heat flux with a Gaussian function of eq. (17).

$$q_a = \eta\frac{VI}{2\pi\sigma^2}\exp\left(-\frac{x^2+y^2}{2\sigma^2}\right) \tag{17}$$

The arc efficiency is assumed to be 0.95. The pressure boundary condition of the arc plasma can be modeled by a Gaussian-like function of eq. (18).

$$P_a = \frac{\mu_0 I^2}{4\pi\sigma^2}\exp\left(-\frac{x^2+y^2}{2\sigma^2}\right) \tag{18}$$

Here, μ_0 denotes the magnetic permeability of free space. Besides the gravitational force, the electromagnetic force that is generated by the electric current density and self-induced magnetic field is considered in eq. (11) as body force. The analytical solutions for the vertical and radial components of the current density and the angular component of the magnetic field are expressed as follows[18]:

$$J_z = \frac{I}{2\pi}\int_0^\infty \lambda J_0(\lambda r)\exp\left(-\lambda^2\sigma^2/4\right)\frac{\sinh[\lambda(c-z)]}{\sinh(\lambda c)}d\lambda \tag{19}$$

$$J_r = \frac{I}{2\pi}\int_0^\infty \lambda J_1(\lambda r)\exp\left(-\lambda^2\sigma^2/4\right)\frac{\cosh[\lambda(c-z)]}{\sinh(\lambda c)}d\lambda \tag{20}$$

$$B_\theta = \frac{\mu_m I}{2\pi}\int_0^\infty J_1(\lambda r)\exp\left(-\lambda^2\sigma^2/4\right)\frac{\sinh[\lambda(c-z)]}{\sinh(\lambda c)}d\lambda \tag{21}$$

Here, J_0 is the first kind of Bessel function of zero order, c is the thickness of the workpiece, z is the vertical distance from the origin, J_1 is the first kind of Bessel function of first order, and μ_m is the magnetic permeability of the material. Next, the buoyancy force, which is a body force, can be modeled by the Boussinesq approximation and is expressed as follows:

$$F_b = \rho g\beta(T-T_0) \tag{22}$$

Here, g is gravity, β is the thermal expansion rate, and T_0 is the reference temperature. Finally, a surface tension model developed for a binary Fe-S system is used to model the Marangoni flow. Thus, the surface tension can be expressed as follows[18]:

$$\gamma(T) = \gamma_m^o - A(T-T_m) - \bar{R}\,T\,\Gamma_s\ln\left(1+k_1 a_i e^{-\Delta H^o/\bar{R}T}\right) \tag{23}$$

where γ_m^o is the surface tension of pure metal at the melting point, A is the negative surface tension gradient for pure metal, T_m is the melting point, Γ_S is the surface excess at saturation, k_1 is the constant related to the entropy of segregation, a_i is the weight percent of sulfur, and ΔH^0 is the standard heat of adsorption. The Gaussian distributed surface heat source effective radius as mentioned in eqs. (17)-(21) was measured from the CCD arc images using abel inversion technique[18].

Figs. 5(a) and (b) describe the molten pool flow patterns between droplet generations in the longitudinal section for a torch angle of -20°. Here the droplet impingent direction is very similar to the molten pool circulation. Thus,

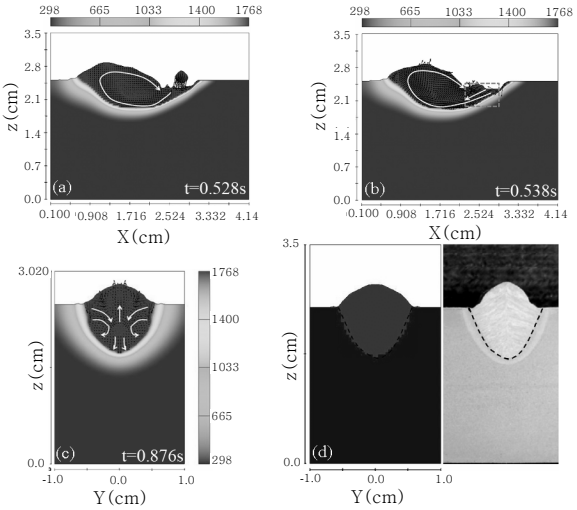

Fig. 5 Calculated temperature profiles and flow patterns for the torch angle of -20° [18]

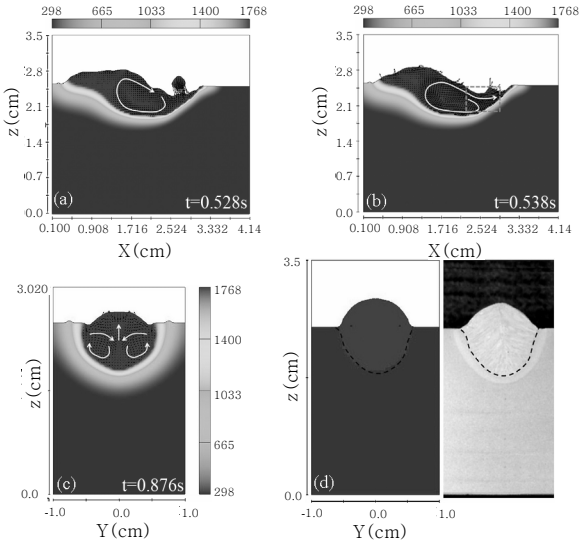

Fig. 6 Calculated temperature profiles and flow patterns for the torch angle of +20° [18]

the momentum can be transferred sufficiently to the weld pool. Specifically, the molten pool flows downward and backward in the dotted box between droplet generations [Fig. 5(b)] just like the droplet impingent moment [Fig. 5(a)], and thus forms a large circulation on a longitudinal cross-section. From Fig. 5(c), it is possible to observe that these flow patterns cause a sharp and deep penetration on a transverse cross-section by convection heat transfer. Figs. 6(a) and (b) depict the molten pool flow patterns between droplet generations in the longitudinal section for a torch angle of +20°. Here the droplet impingent direction does not match the molten pool direction. Therefore, the molten pool can flow forward in the dotted-box shown in Fig. 6(b) while it flows backward at -20° case. With these flow patterns, less momentum can be transferred compared to -20° case, which results in a relatively small molten pool circulation on a longitudinal cross-section, and induces a shallow penetration, as shown in Fig. 6(c). Finally, the numerical models are validated by comparing the simulation results with the experimental ones, as shown in Figs. 5(d) and 6(d).

Cho et al.[19] simulated the heat transfer and fluid flow in two wire tandem SAW process for two cases. In case 1 the current values for the leading and trailing arcs are 700 A and 1000 A, respectively, and the welding speed is 22.8 mm/s. In case 2 the leading and trailing arcs current values are 1000 A and 700 A, respectively, 22.6 mm/s and the welding speed is 26.8 mm/s. In both the cases, heat input is 2.5 kJ/mm. Fig. 7 depict the temperature distribution and molten pool flow for case 1. The lower current of the leading arc reduce the corresponding stiffness and increase its displacement. As a result the droplets, arc heat, and arc forces from the leading electrode cannot be focused on a similar weld pool spot, but the droplets disperse forward or backward of welding direction and then form the volume of the molten pool ahead of the leading electrode. With these fluid behaviors, the molten pool can fill in the V-groove even

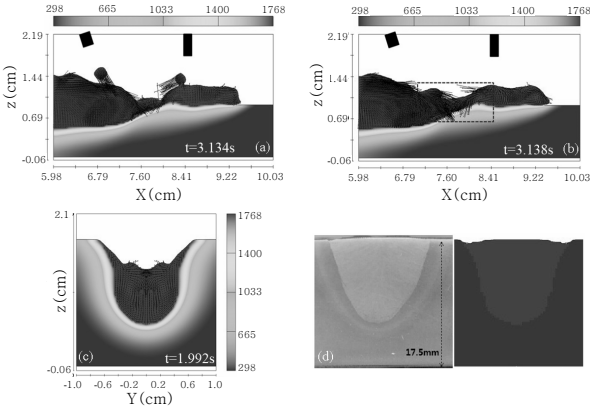

Fig. 7 Calculated temperature profiles and flow patterns in case 1[19]

though the leading electrode has not yet approached the spot. Consequently, the free surface location of z-direction during the droplet impingement is higher than the initial V-groove point, so the molten pool penetrates to a lesser degree. In the longitudinal section as shown in Figs. 7(b), the molten pool cannot flow downward sufficiently and circulate counterclockwise in a dotted-box; therefore, this molten fluid produces a bowl-shaped weld bead that shows a relatively shallow weld bead [Fig. 7(c)].

Fig. 8 depict the temperature distribution and molten pool flow for case 2. For this welding condition, the arc center displacement of the leading electrode is very small, as a result the arc heat, arc force and droplet impingement can be focused under the leading electrode. Therefore, the volume of molten pool ahead of the leading electrode is very small because droplets do not fly ahead of the leading electrode as shown in Fig. 8. In the transverse section, droplets from the leading electrode impinge on the weld pool whose height is lower than the initial V-groove point; thus, the deep penetration can be formed as shown in Fig. 8(a). Moreover, the weld pool flows long after droplet impingement in the longitudinal section as shown in Fig. 8(b), so this can be another reason to make the deep penetration due to the dynamic convection heat transfer. Further the voltage values significantly affects the arc size and the resultant bead width; therefore, when the trailing electrode reaches the weld pool, the penetration is very slightly increased as shown in the dotted-circle of Fig. 8(c) while the bead width becomes wider because a higher voltage value can produce a large size of arc plasma. The computed weld pool profiles are found to be in fair agreement with the corresponding experimental results in both the cases.

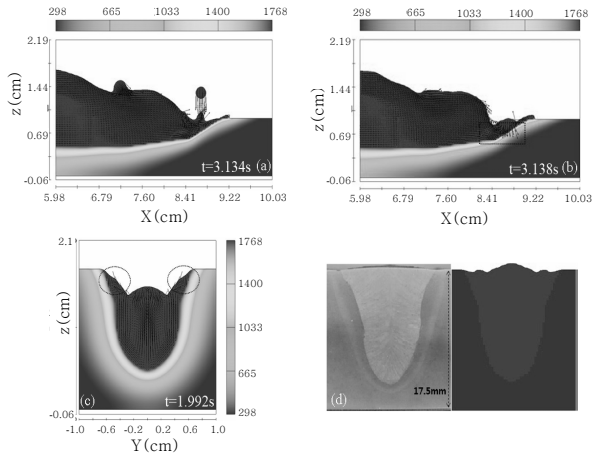

Fig. 8 Calculated temperature profiles and flow patterns in case 2[19)]

3. Conclusions

A brief review of the numerical studies on the single wire and multi-wire SAW processes is the focus of the present paper. The conduction heat transfer analysis, and the heat transfer and fluid flow analysis in the SAW processes are reviewed. Some of the salient points in the present review are summarized as below.

- In a conduction based numerical analysis, double-ellipsoidal volumetric heat source model can numerically account for the heat transport inside the weld pool and hence it is preferred over the Gaussian distributed surface heat source to simulate the heat transfer from the welding arc.
- Analytical models to predict the volumetric heat source dimensions are developed as a function of the groove dimensions and the welding conditions.
- The conduction heat transfer models are unable to account for convective transport of heat, which is especially significant in large weld pool in a true sense. Heat transfer and fluid flow modeling of the welding process is required for the reliable prediction of the single and multi-wire SA weld dimensions and temperature distribution.

Acknowledgements

The authors gratefully acknowledge the support of the Brain Korea 21 plus project, Korean Ministry of Knowledge Economy (No.2013-10040108) and Mid-career 363 Researcher Program through NRF (2013-015605).

References

1. S. A. David and T. DebRoy : Current issues and problems in welding science, Science, **257-5096** (1992), 497-502
2. A. K. Pathak and G. L. Datta : Three-dimensional finite element analysis to predict the different zones of microstructure in submerged arc welding, proceedings of the institution of mechanical engineers, **218-3** (2004), 269-280
3. M. M. Mahapatra, G. L. Datta, B. Pradhan and N. R. Mandal : Three-dimensional finite element analysis to predict the effects of SAW process parameters on temperature distribution and angular distortion in single-pass butt joints with top and bottom reinforcements, International journal of pressure vessels and piping, **83-7** (2006), 721-729
4. P. Biswas, M. M. Mahapatra and N. R. Mandal : Numerical and experimental study on prediction of thermal history and residual deformation of double-sided fillet welding, Proceedings of the Institution of Mechanical Engineers: Part B Journal of Engineering Manufacture, **224-1** (2010), 125-134
5. J. Goldak, A. Chakravarti and M. Bibby : A new finite element model for welding heat source, Metallurgical Transactions B, **15-2** (1984), 299-305
6. D. Gery, H. Long and P. Maropoulos : Effect of welding speed, energy input and heat source distribution on temperature variations in butt welding, Journal of Materials Processing Technology, **167-8** (2005), 393-401
7. E. A. Bonifaz : Finite element analysis of heat flow in single pass arc welding, Welding Journal, **79-5** (2005), 121s-125s
8. T. W. Eagar and N. S. Tsai : Temperature fields produced by traveling distributed heat sources, Welding Journal, **62-12** (1983), 346s-355s
9. A. Sharma, A. K. Chaudhary, N. Arora and B. K. Mishra : Estimation of heat source model parameters for twin wire submerged arc welding, International Journal of Advanced Manufacturing Technology, **45** (2009), 1096-1103
10. D. V. Kiran, B. Basu, A. K .Shah, S. Mishra and A. De : Three dimensional heat transfer analysis of two wire tandem submerged arc welding, ISIJ International, **515** (2011), 793-798
11. W. G. Essers and R.Walter : Heat transfer and penetration mechanisms with GMA and plasma-GMA welding, Welding Journal, **60-2** (1981), 37s-42s
12. J. F. Lancaster : The physics of welding, Pergamon Press, New York, NY, 1984
13. D. V. Kiran, B. Basu, A. K. Shah, S. Mishra and A. De : Probing influence of welding current on weld quality in two wire tandem submerged arc welding of HSLA steel, Science and Technology of Welding and Joining, **15-2** (2010), 111-116
14. Y. Yang : The effect of submerged arc welding parameters on the properties of pressure vessel and wind turbine tower steels, M.S thesis, University of Saskatchewan, Saskatoon, 2008
15. G. M. Reddy and P. K. Ghosh : The influence of electrode polarity and welding current on mechanical properties of submerged arc weld (SAW) in C-Mn steels, Indian Welding Journal, **26-3** (1993), 1-4
16. A. Pilipenko : Computer simulation of residual stress and distortion of thick plates in multielectrode submerged arc welding their mitigation techniques, Ph.D. thesis, Nowegian University of Science and Technology, Norway, 2001
17. S. Kou : Welding metallurgy, A Wiley-Interscience publication, New Jersey, 2003
18. D. W. Cho, W. H. Song, M. H. Cho and S. J. Na : Analysis of submerged arc welding process by three-dimensional computational fluid dynamics simulation, Journal of Materials Processing Technology, **213-12** (2013), 2278-2291
19. D. W. Cho, D. V. Kiran and S. J. Na : Molten pool behavior in the tandem submerged arc welding process, Journal of Materials Processing Technology, **214-11** (2014), 2233-2247

Degala Ventaka Kiran received the B.E. degree in mechanical engineering from Andhra University, Visakhapatnam, India, in 2005, M.Tech degree in mechanical and industrial engineering from IIT Roorkee, Roorkee, India in 2007 and the Ph.D. degree in mechanical engineering from IIT Bombay, Mumbai, India in 2012.

He is a Post doctoral researcher with the Advanced Laser, Plasma and Hybrid Applications Lab, Korea Advanced Institute of Science and Technology, Daejeon, Korea. His current research interests include Weldig Science and Technology, numerical analysis of heat transfer and fluid flow, residual stress and deformation in fusion welding processes, experimental stress analysis, and statistical modeling and optimization.

Suck-Joo Na graduated from Seoul National University for B.Sc. and Korea Advanced Institute of Science and Technology for M.Sc. in Mechanical Engineering, and has got his Dr.-Ing. degree from the Welding and Joining Institute of TU Braunschweig, Germany.

Professor Na is working at KAIST, Korea for more than 30 years, educating and researching in the analysis, optimization and automation of welding processes and laser materials processing. Professor Na is one of the leading scientists in the field of process simulation of arc and laser beam welding, most notably of laser hybrid welding, in which he links his expertise of arc physics and multiple reflections in the keyhole with that of weld pool dynamics during arc and laser welding. He has published 236 research papers in SCI and Korean

domestic journals, and presented more than 230 papers at international and domestic conferences.

Professor Na has been awarded various prizes from Korean Welding and Joining Society (KWJS), American Welding Society (AWS) such as excellent scientific research award, best paper award and Charles H. Jennings Memorial Award. He was elected as the fellow of AWS in 2005, as the member of the National Academy of Engineering of Korea in 2007 and as the fellow of the Korean Academy of Science and Technology in 2008. Recently he was selected as the FiDiPro Professor to establish a digital welding research group at VTT in Finland from 2014 to 2016.

After serving as a member of the board of directors of KWJS, Professor Na was the president of KWJS from 2007 to 2008, a member of Technical Management Board of IIW from 2010 to 2012 and is now serving as the president of Asian Welding Federation.